Hamburger Beiträge
zur Angewandten Mathematik

POD Model Order Reduction of Drift-Diffusion Equations in Electrical Networks

Michael Hinze, Martin Kunkel and Morten Vierling

POD Model Order Reduction of Drift-Diffusion Equations in Electrical Networks

Michael Hinze, Martin Kunkel and Morten Vierling

Abstract We consider integrated circuits with semiconductors modelled by modified nodal analysis and 1D drift-diffusion equations. The drift-diffusion equations are discretized in space using finite element methods. The discretization yields a high dimensional differential-algebraic equation. We show how POD methods can be used to reduce the dimension of the model. We compare reduced and fine models and give numerical results for a basic network with one diode. Furthermore we discuss an adaptive approach to construct POD models which are valid our certain parameter ranges. Finally, numerical investigations for the reduction of a 4-diode rectifier network are presented, which clearly indicate that POD model reduction delivers surrogate models for the diodes involved, which depend on the position of the semiconductor in the network.

1 Introduction

In this article we investigate a POD-based model order reduction for semiconductors in electrical networks. Electrical networks can be efficiently modelled by a differential-algebraic equation (DAE) which is obtained from modified nodal analysis. Denoting by e the node potentials and by j_L and j_V the currents of inductive and voltage source branches, the DAE reads (see [14])

Michael Hinze · Martin Kunkel · Morten Vierling
Department of Mathematics, University of Hamburg, Bundesstr. 55, 20146 Hamburg, Germany, e-mail: michael.hinze@uni-hamburg.de, e-mail: kunkel@math.uni-hamburg.de, e-mail: vierling@math.uni-hamburg.de

$$A_C \frac{d}{dt} q_C(A_C^\top e, t) + A_R g(A_R^\top e, t) + A_L j_L + A_V j_V = -A_I i_s(t), \qquad (1)$$

$$\frac{d}{dt} \phi_L(j_L, t) - A_L^\top e = 0, \qquad (2)$$

$$A_V^\top e = v_s(t). \qquad (3)$$

Here, the incidence matrix $A = [A_R, A_C, A_L, A_V, A_I]$ represents the network topology and q_C, g and ϕ_L are continuously differentiable functions defining the voltage-current relations of the network components. The continuous functions v_s and i_s are the voltage and current sources. For example consider the network in Figure 1. Under the assumption that the Jacobians

$$D_C(e, t) := \frac{\partial q_C}{\partial e}(e, t), \quad D_G(e, t) := \frac{\partial g}{\partial e}(e, t), \quad D_L(j, t) := \frac{\partial \phi_L}{\partial j}(j, t)$$

are positive definite, analytical properties (e.g. the index) of DAE (1)-(3) are investigated in [2] and [3]. In linear networks, the matrices D_C, D_G and D_L are positive definite diagonal matrices with capacitances, resistances and inductances on the diagonal.

Often semiconductors themselves are modelled by electrical networks. These models are stored in a library and are stamped into the surrounding network in order to create a complete model of the integrated circuit. Here we use a different approach which uses the transient drift-diffusion equations as a model for semiconductors. Advantages are the higher accuracy of the model and fewer model parameters. On the other hand, numerical simulations are more expensive. For a comprehensive overview of the drift-diffusion equations we refer to [7]. Using the notation introduced there we have the following system of partial differential equations for the electrostatic potential ψ, the electron and hole concentrations n and p and the current densities J_n and J_p:

$$\begin{aligned}
\text{div}(\varepsilon \, \text{grad} \, \psi) &= q(n - p - C), \\
-q \partial_t n + \text{div} J_n &= q R(n, p, J_n, J_p), \\
q \partial_t p + \text{div} J_p &= -q R(n, p, J_n, J_p), \\
J_n &= \mu_n q (U_T \, \text{grad} \, n - n \, \text{grad} \, \psi), \\
J_p &= \mu_p q (-U_T \, \text{grad} \, p - p \, \text{grad} \, \psi).
\end{aligned}$$

The nonlinear function R describes the rate of electron/hole recombination, q is the elementary charge, ε the dielectricity, μ_n and μ_p are the mobilities of electrons and holes. The temperature is assumed to be constant which leads to a constant thermal voltage U_T. The function C is the doping profile. Additionally there are boundary conditions for n, p, J_n and/or J_p which depend on the type of contact (e.g. Ohmic contacts, Schottky contacts).

The coupling between drift-diffusion equations and the electrical network yields a partial differential-algebraic equation (PDAE). The analytical and numerical analysis of such systems is subject to current research, see [1, 5, 12, 14].

This paper is organized as follows. In Section 2 we present the model for the complete coupled system, meaning the network including semiconductors. The coupled model then is simulated using finite-element methods in Section 3. This gives us so-called snapshots $y_i := y(t_i)$, $i = 1, \ldots, k$, which represent the state of the circuit and the semiconductors at time t_i. Based on these snapshots and POD we construct a reduced model in Section 4. A numerical investigation of the model is presented in Section 5 where also advantages and shortcomings of our approach are discussed.

2 Complete coupled system

In the present section we develop the complete system in 1D. The n_s semiconductors are diodes with length L_k, $k = 1, \ldots, n_s$. For the sake of simplicity we assume that the contacts are Ohmic, and that the dielectricities ε_k are constant over the whole domain $\Omega := [0, L_k]$. Furthermore we focus on the Shockley-Read-Hall recombination

$$R(n, p) = \frac{np - \eta^2}{\tau_p(n + \eta) + \tau_n(p + \eta)}$$

which does not depend on the current densities. Here, η denotes the intrinsic concentration, τ_n and τ_p are the average lifetimes of electrons and holes.

The simulation of the complete coupled system is expensive and numerically difficult due to bad scaling of the drift-diffusion equations. The numerical issues can be significantly reduced by the unit scaling procedure discussed in [10], e.g. by substituting

$$x = L\tilde{x}, \quad \psi = U_T\tilde{\psi}, \quad n = \|C\|_\infty \tilde{n}, \quad p = \|C\|_\infty \tilde{p}, \quad C = \|C\|_\infty \tilde{C},$$

$$J_n = \frac{qU_T\|C\|_\infty \mu_n}{L}\tilde{J}_n, \quad J_p = \frac{qU_T\|C\|_\infty \mu_p}{L}\tilde{J}_p, \quad \eta = \tilde{\eta}\|C\|_\infty.$$

The scaled complete coupled system is constructed as follows. (We neglect the tilde-sign over the scaled variables.) Let j_S be the currents through the diodes. Consequently, a term $A_S j_S$ is added in equation (1), e.g.

$$A_C\frac{d}{dt}q_C(A_C^\top e, t) + A_R g(A_R^\top e, t) + A_L j_L + A_V j_V + A_S j_S = -A_I i_s(t), \quad (4)$$

$$\frac{d}{dt}\phi_L(j_L, t) - A_L^\top e = 0, \quad (5)$$

$$A_V^\top e = v_s(t). \quad (6)$$

The voltage-current relation for the semiconductor k is established by the couplings

$$j_{S,k}(t) = \frac{aqU_T\|C\|_\infty}{L}\left(\mu_n J_n(t,1)+\mu_p J_p(t,1)\right) - \frac{a\varepsilon U_T}{L}\frac{\partial}{\partial t}\frac{\partial \psi}{\partial x}(t,1), \qquad (7)$$

$$\psi(t,0) = 0, \qquad (8)$$

$$\psi(t,1) = \frac{A_{S,k}^\top e(t)+\psi_{bi}}{U_T}, \qquad (9)$$

where a is the size of the contact of the diode and ψ_{bi} is the build-in potential. Equation (7) states that the current is the integral of the total current density over the interface area. In order to simplify the presentation, we neglect the index k for the semiconductors wherever possible. The scaled drift-diffusion equations for each semiconductor now read

$$\lambda\,\partial_{xx}\psi = n-p-C, \qquad (10)$$

$$-\partial_t n + v_n\partial_x J_n = R(n,p), \qquad (11)$$

$$\partial_t p + v_p\partial_x J_p = -R(n,p), \qquad (12)$$

$$J_n = \partial_x n - n\partial_x\psi, \qquad (13)$$

$$J_p = -\partial_x p - p\partial_x\psi \qquad (14)$$

with $\lambda := \frac{\varepsilon U_T}{L^2 q\|C\|_\infty}$, $v_n := \frac{U_T\mu_n}{L^2}$ and $v_p := \frac{U_T\mu_p}{L^2}$. Finally we have the boundary values at the Ohmic contacts

$$n(t,0) = \frac{1}{2}\left(\sqrt{C(0)^2+4\eta^2}+C(0)\right), \quad n(t,1) = \frac{1}{2}\left(\sqrt{C(1)^2+4\eta^2}+C(1)\right),$$

$$p(t,0) = \frac{1}{2}\left(\sqrt{C(0)^2+4\eta^2}-C(0)\right), \quad p(t,1) = \frac{1}{2}\left(\sqrt{C(1)^2+4\eta^2}-C(1)\right).$$
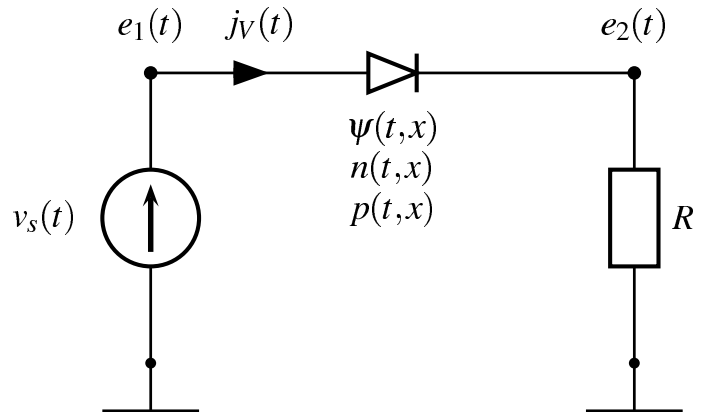
Fig. 1 Basic test circuit with one diode. The network is described by

$$A_V = \begin{pmatrix} 1, & 0 \end{pmatrix}^\top,$$
$$A_S = \begin{pmatrix} -1, & 1 \end{pmatrix}^\top,$$
$$A_R = \begin{pmatrix} 0, & 1 \end{pmatrix}^\top,$$
$$g(A_R^\top e,t) = \frac{1}{R}e_2(t).$$

3 Simulation of the full system

Classical approaches for simulation of drift-diffusion equations (e.g. Gummel iterations [4]) approximate J_n and J_p by piecewise constant functions and then solve equations (13) and (14) with respect to n and p explicitly. This helps reducing the computational effort and increases the numerical stability. For the proposed model order reduction this method admits the disadvantage, that it introduces additional non-linearities, since the discrete solution of (13) and (14) is build up in terms of $\exp \psi$, see [12].

Here we consider two finite element approaches to the drift-diffusion equations, namely standard Galerkin and mixed finite element methods. We start with a standard Galerkin approach. For the sake of simplicity we use an equally distributed finite element mesh with N elements and mesh width $h := 1/N$. The functions ψ, n and p are approximated by piecewise linear and globally continuous functions, J_n and J_p are approximated by piecewise constant functions, e.g.

$$\psi(t,x) := \sum_{i=0}^{N} \psi_i(t)\phi_i(x), \quad n(t,x) := \sum_{i=0}^{N} n_i(t)\phi_i(x), \quad p(t,x) := \sum_{i=0}^{N} p_i(t)\phi_i(x),$$

$$J_n(t,x) := \sum_{i=1}^{N} J_{n,i}(t)\varphi_i(x), \quad J_p(t,x) := \sum_{i=1}^{N} J_{p,i}(t)\varphi_i(x),$$

where the functions $\{\phi_i\}$ and $\{\varphi_i\}$ are the corresponding ansatz or trial functions. For ψ, n and p only the interior coefficients, e.g. $\psi(t) = (\psi_1, \ldots, \psi_{N-1})^\top$, are variable, the coefficients corresponding to the boundary elements are given by the Dirichlet boundary conditions. Note that the time is not discretized at this point which refers to the so-called method of lines. The finite element method leads to the following DAE for the unknown vector-valued functions of time ψ, n, p, J_n, J_p for each semiconductor:

$$0 = \lambda S\psi(t) + Mn(t) - Mp(t) - C_h + b_\psi(e(t)),$$
$$-M\dot{n}(t) = -v_n D^\top J_n(t) + hR(n(t), p(t)),$$
$$M\dot{p}(t) = -v_p D^\top J_p(t) - hR(n(t), p(t)), \tag{15}$$
$$0 = hJ_n(t) + Dn(t) - \text{diag}\left(Bn(t) + \tilde{b}_n\right) D\psi(t) + b_n,$$
$$0 = hJ_p(t) - Dp(t) - \text{diag}\left(Bp(t) + \tilde{b}_p\right) D\psi(t) + b_p,$$

where $S, M \in \mathbb{R}^{(N-1)\times(N-1)}$ and $D, B \in \mathbb{R}^{N\times(N-1)}$ are assembled finite element matrices. The vectors $b_\psi(e(t))$, b_n, $\tilde{b}_n$, b_p and $\tilde{b}_p$ implement the boundary conditions imposed on ψ, n and p, which are given by

$$\psi_0(t) = 0, \qquad\qquad \psi_N(t) = \frac{A_{S,k}^\top e(t) + V_{bi}}{U_T},$$

$$n_0(t) = \frac{1}{2}\left(\sqrt{C(0)^2 + 4\eta^2} + C(0)\right), \quad n_N(t) = \frac{1}{2}\left(\sqrt{C(1)^2 + 4\eta^2} + C(1)\right),$$

$$p_0(t) = \frac{1}{2}\left(\sqrt{C(0)^2 + 4\eta^2} - C(0)\right), \quad p_N(t) = \frac{1}{2}\left(\sqrt{C(1)^2 + 4\eta^2} - C(1)\right).$$

Discretization of the coupling condition for the current completes the discretized system:

$$j_{S,k}(t) = \frac{aqU_T\|C\|_\infty}{L}\left(\mu_n J_{n,N}(t) + \mu_p J_{p,N}(t)\right) - \frac{a\varepsilon U_T}{Lh}\left(\dot\psi_N(t) - \dot\psi_{N-1}(t)\right),$$

Supposing that the fluxes J_n and J_p as well as the gradient of ψ play a dominant role in (10)-(14) one might argue, that they should be resolved better, than as piecewise constant functions. This directly leads to the Raviart-Thomas finite element approach, where the concentrations n and p and the potential ψ are approximated by piecewise constant functions, but the fluxes $\nabla\psi$, J_n and J_p are elements of the Raviart-Thomas space of order zero. In one space dimension, the Raviart-Thomas approach leads to piecewise linear, continuous approximations to these functions, so that the ansatz space is just $\mathrm{span}\{\phi_0,\dots,\phi_N\}$. The ansatz space for ψ, n and p is given by $\mathrm{span}\{\varphi_1,\dots,\varphi_N\}$. The idea is now not to discretize (10)-(14) separately, but instead to discretize variable-flux pairs together. For example the equations (11,13)

$$-\partial_t n + v_n \partial_x J_n = R(n,p),$$
$$J_n = \partial_x n - n\partial_x\psi,$$

define the variable n and its flux J_n. The first equation is tested with φ, the second is tested with ϕ and integrated by parts to obtain

$$-\int_\Omega \partial_t n\varphi + v_n\int_\Omega \varphi\partial_x J_n = \int_\Omega R(n,p)\varphi,$$
$$\int_\Omega J_n\phi = -\int_\Omega n\partial_x\phi - \int_\Omega n\partial_x\psi + [n\phi]_0^1.$$

This formulation avoids derivatives of n. The pairs of equations (12,14) and (10,16) are treated in a similar way. By using $\{\varphi_i\}$ and $\{\phi_i\}$ as test and trial functions and by substituting $\partial_x\psi$ by

$$g_\psi = \partial_x\psi, \tag{16}$$

we arrive at the following finite dimensional system of equations:

$$0 = \lambda D g_\psi(t) + h n(t) - h p(t) + \hat{C}_h$$
$$h \dot{n}(t) = \nu_n D J_n(t) + h R(n(t), p(t))$$
$$h \dot{p}(t) = \nu_p D J_p(t) + h R(n(t), p(t))$$
$$0 = \quad D^\top \psi(t) + M g_\psi(t) - \hat{b}_\psi(e(t))$$
$$0 = -D^\top n(t) + M J_n(t) + \text{diag}\left(\hat{B} g_\psi(t)\right) n(t) - \hat{b}_n$$
$$0 = -D^\top p(t) + M J_p(t) + \text{diag}\left(\hat{B} g_\psi(t)\right) p(t) - \hat{b}_p$$

with sparse matrices $D \in \mathbb{R}^{N \times (N+1)}$, $M \in \mathbb{R}^{(N+1) \times (N+1)}$ and $\hat{B} \in \mathbb{R}^{N \times (N+1)}$ and vectors $\hat{C}_h \in \mathbb{R}^N$ and $\hat{b}_\psi(e(t)), \hat{b}_n, \hat{b}_p \in \mathbb{R}^{N+1}$.

The discretized equations are implemented in MATLAB, and the DASSL software package [9] is used to integrate the high dimensional DAE. Initial values are stationary states obtained by setting all time derivatives to 0. A basic test circuit with one diode is depicted in Figure 1, where the model parameters are presented in Table 1. The input $v_s(t)$ is chosen to be sinusoidal with amplitude $5V$. The numerical results in Figure 2 show the capacitive effect of the diode for high input frequencies. Similar results are obtained in [11] using the simulator MECS.

Table 1 Diode model parameters.

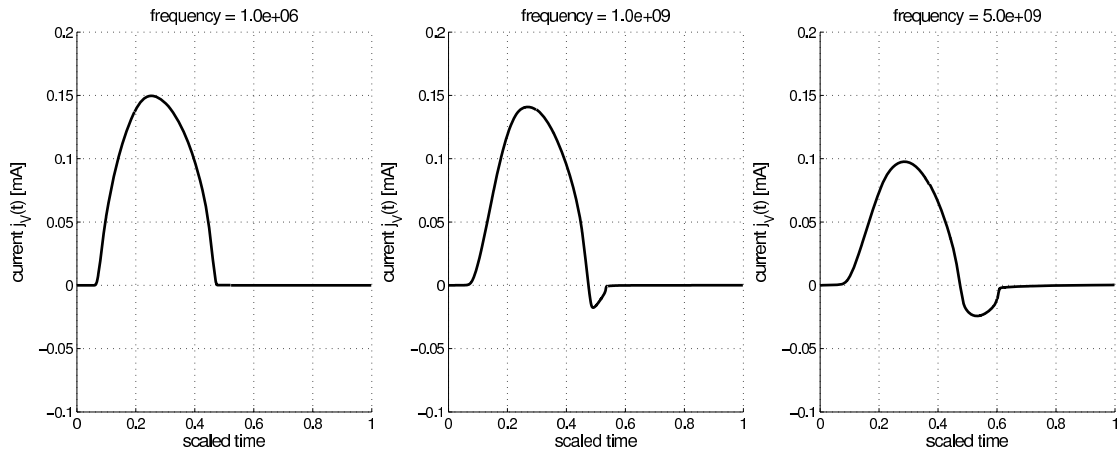| Parameter	Value		Parameter	Value	
L	10^{-4}	$[cm]$	ε	$1.03545 \cdot 10^{-12}$	$[F/cm]$
U_T	0.0259	$[V]$	η	$1.4 \cdot 10^{10}$	$[1/cm^3]$
μ_n	1350	$[cm^2/(Vsec)]$	τ_n	$330 \cdot 10^{-9}$	$[sec]$
μ_p	480	$[cm^2/(Vsec)]$	τ_p	$33 \cdot 10^{-9}$	$[sec]$
a	10^{-5}	$[cm^2]$	$C(x), x < L/2$	$-9.94 \cdot 10^{15}$	$[1/cm^3]$
			$C(x), x \geq L/2$	$4.06 \cdot 10^{18}$	$[1/cm^3]$

Fig. 2 Current j_V through the basic network for input frequencies 1 MHz, 1 GHz and 5 GHz. The capacitive effect is clearly demonstrated.

4 Model reduction

Now we want to reduce the computational effort of repeated dynamical simulations by applying proper orthogonal decomposition (POD) to the drift-diffusion equations. The POD reduction procedure is formulated in the Appendix, and from here onwards is used with $X := L^2(\Omega)$. As an example we discuss the reduction based on the standard finite element approximation (15), Raviart-Thomas elements are treated analogously.

The test functions for a standard Dirichlet problem are expected to vanish at the boundary. Hence, in the standard finite element case, before performing the POD of the state space, we relate the solution to a reference state (not necessarily a solution), e.g. a stationary solution or a mean value, that fulfills the boundary conditions. The functions

$$\tilde{\psi} = \psi - \psi_r \,,\; \tilde{n} = n - n_r \,,\; \tilde{p} = p - p_r$$

then satisfy homogeneous boundary conditions. The reference ψ_r is an exception in so far, that in general it cannot be a stationary state, since ψ underlies varying boundary conditions. Here, we use the stationary state, scaled in such a way that the boundary conditions are satisfied, e.g.

$$\psi_r(t,x) = \frac{\psi(t,1)}{\psi(t_0,1)} \psi_r(t_0,x) = \frac{A_S^\top e(t) + \psi_{bi}}{A_S^\top e(t_0) + \psi_{bi}} \psi_r(t_0,x).$$

We further set

$$\tilde{J}_n = J_n - J_n^r \,,\; \tilde{J}_p = J_p - J_p^r \,.$$

In the case of the Raviart-Thomas approach the relation to a reference state is not necessary, since the boundary values are included more naturally through the variational formulation.

The time-snapshot POD procedure described in the Appendix delivers Galerkin ansatz spaces for $\tilde{\psi}$, $\tilde{n}$, $\tilde{p}$, $\tilde{J}_n$ and $\tilde{J}_p$. This leads to the ansatz

$$\begin{aligned}
\psi^{POD}(t) &= \psi_r(t) + U_\psi H_\psi(t)\,, \\
n^{POD}(t) &= n_r(t) + U_n H_n(t)\,, \quad p^{POD}(t) = p_r(t) + U_p H_p(t)\,, \\
J_n^{POD}(t) &= J_n^r(t) + U_{J_n} H_{J_n}(t)\,, \quad J_p^{POD}(t) = J_p^r(t) + U_{J_p} H_{J_p}(t)\,.
\end{aligned}$$

The matrices

$$\begin{aligned}
U_\psi \in \mathbb{R}^{(N-1) \times k_\psi}\,,\; U_n &\in \mathbb{R}^{(N-1) \times k_n}\; U_p \in \mathbb{R}^{(N-1) \times k_p} \\
U_{J_n} &\in \mathbb{R}^{N \times k_{J_n}}\,,\quad U_{J_p} \in \mathbb{R}^{N \times k_{J_p}}\,,
\end{aligned}$$

contain the POD-functions as columns as in Equation (17), the vectors $H_{(.)}$ the corresponding time-variant coefficients. The number $k_{(.)}$ is the respective number of POD basis functions included. Assembling the POD system then leads to a DAE system similar to (15),

$$0 = \lambda \tilde{S} H_\psi + U_\psi^\top \left(M(U_n H_n - U_p H_p) - C_h \right) + c_1 + \tilde{c}_1(e),$$

$$-\tilde{M}_{nn} \dot{H}_n = -\nu_n \tilde{D}_n^\top H_{J_n} + h U_n^\top R\left(n_r + U_n H_n, p_r + U_p H_p \right) + c_2,$$

$$\tilde{M}_{pp} \dot{H}_p = -\nu_p \tilde{D}_p^\top H_{J_p} - h U_p^\top R\left(n_r + U_n H_n, p_r + U_p H_p \right) + c_3,$$

$$0 = h H_{J_n} + \tilde{D}_n H_n + \mathbf{B}(H_n, H_\psi) + L_n H_\psi + c_4,$$

$$0 = h H_{J_p} - \tilde{D}_p H_p + \mathbf{B}(H_p, H_\psi) + L_p H_\psi + c_5.$$

Here

$$\tilde{S} = U_\psi^\top S U_\psi, \quad \tilde{M}_{nn} = U_n^\top M U_n, \quad \tilde{M}_{pp} = U_p^\top M U_p,$$
$$\tilde{D}_n = U_{J_n}^\top D U^n, \quad \tilde{D}_p = U_{J_p}^\top D U^p,$$

where the matrices M, S, and D and the vector C_h are the same as in equation (15). The constant vectors c_i and matrices L_n, L_p arise from the reference states, and can be computed offline together with the other matrices and the bi-linear map $\mathbf{B}$; c_2 and c_3 vanish in case of stationary reference states n_r and p_r. The vector $\tilde{c}_1(e(t))$ includes the boundary condition on ψ.

5 Numerical investigation

Figure 3 shows the development of the error between the reduced and the unreduced numerical solutions, plotted over the neglected information Δ (see (18)), which is measured by the relative error between the non-reduced states ψ, n, p, J_n, J_p and their projections onto the respective reduced state space. The number of POD basis functions for each variable is chosen so that the indicated approximation quality is reached, i. e.

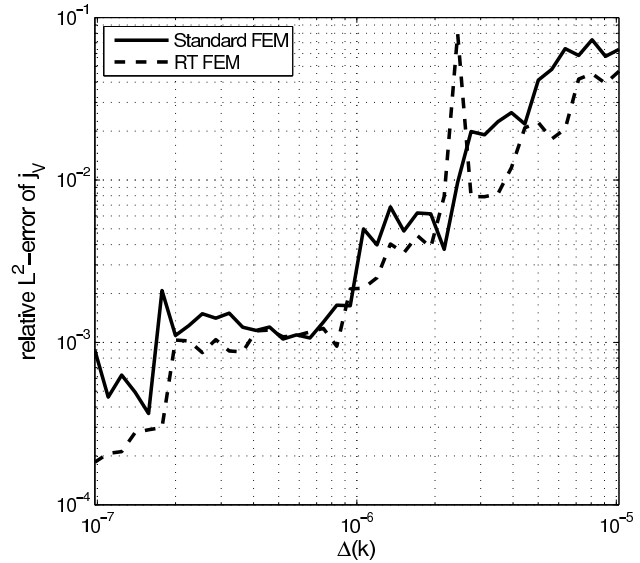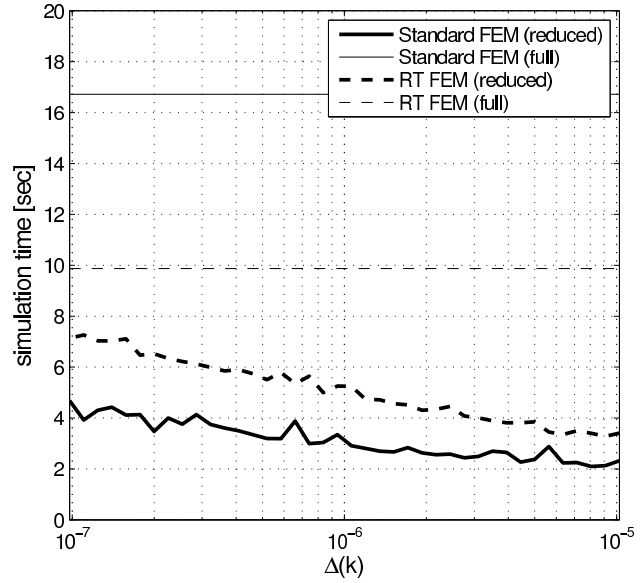$$\Delta := \Delta_\psi \simeq \Delta_n \simeq \Delta_p \simeq \Delta_{J_n} \simeq \Delta_{J_p}.$$

Fig. 3 L_2 error of j_V for standard and Raviart-Thomas FEM.

Fig. 4 Time consumption for simulation runs for Figure 3. The fine lines indicate the time consumption for the simulation of the original full system.

Since we compute all POD basis functions anyway, this procedure does not involve any additional costs.

In Figure 4 the simulation times are plotted versus the neglected information Δ. As one can see, the simulation based on standard finite elements takes twice as long as that based on RT elements. However, this difference is not observed for the simulation of the corresponding reduced models.

The whole POD approach in the present situation makes sense only, if the singular values would decay rapidly. Else one would have to use too many POD basis functions and would end up with a rather large and dense POD Galerkin system. To illustrate, that the singular values are indeed decaying exponentially, Figure 5 shows the total number of singular vectors $k = k_\psi + k_n + k_p + k_{J_n} + k_{J_p}$ required to undercut
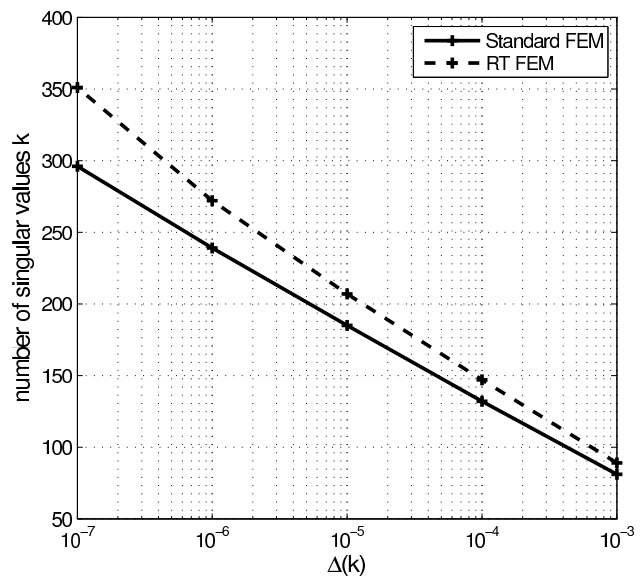

Fig. 5 The number of required singular values grows only logarithmically with the requested accuracy.
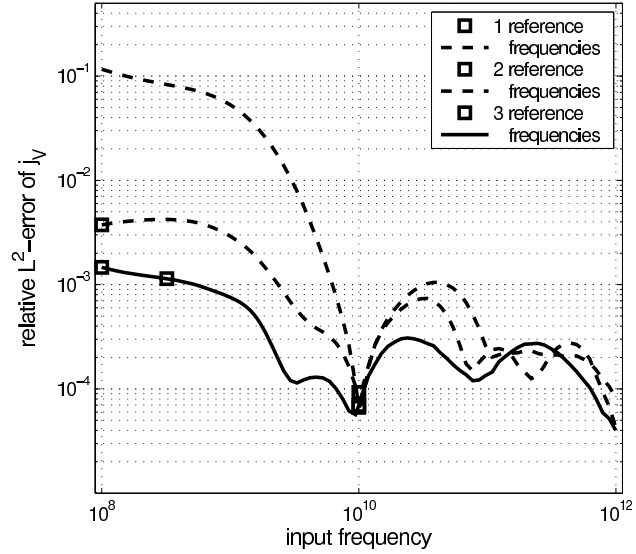
Fig. 6 Reduction error plotted over the frequency parameter space. The reduced model was created with 1 to 3 reference frequencies.

a given state space cut-off error Δ. While the number of singular vectors included increases only linearly, the cut-off error tends to zero exponentially.

Although POD model order reduction often works well, it is clearly a drawback of the method that the reduced system depends on the inputs and on the parameters of the system under consideration. A possible remedy consists in performing simulations over a certain input and/or parameter range and then to collect all simulations in a global snapshot matrix $Y := [Y^1, Y^2, \ldots]$. Here, each Y^i represents the snapshots taken for a certain input/parameter pair. In this context now the question pops up which inputs/parameters to choose in order to obtain a reduced model, which is valid over the whole input/parameter range. Let us elaborate on this complex of questions with the following example.

For the basic circuit we choose the frequency of the input voltage v_s as parameter. Let the parameter space be the interval $[10^8 \text{Hz}, 10^{12} \text{Hz}]$. We start the investigation with a reduced model where the snapshot matrix is created from the simulation of the full model at a frequency of 10^{10} Hz. The difference between simulations of the full model and the reduced model is the reduction error plotted in Figure 6 (dotted line). A second reduced model is constructed by adding snapshots from the full simulation at a frequency of 10^8 Hz, which is the frequency for which the error is maximal. Note that we do not alter the number of singular values for the second model. One can see that the error is significantly reduced in the second model (dashed line). A third model is constructed analogously (solid line).

Of course this adaptive reduction method is only academical, since it is based on full model integrations over the whole parameter space. For practical purposes we will need to develop a-posterior error estimators in the parameter space. It may be possible to apply the methods of [8] to the problem under consideration. In the present situation also a parameter POD along the lines of [6] could be applied. The parameter snapshots are chosen as simulations of the quasi-stationary drift-diffusion model related to the respective parameter value (here: frequency of voltage source).

Finally we note that the presented reduction method does not create reduced models for semiconductors as such, but accounts for the position of the semiconductors in a given network. The modes or POD basis functions of two identical semiconductors may be different due to their different operating states. To demonstrate this fact, we consider the rectifier network in Figure 7 and measure the distance between the spaces U^1 and U^2 which are spanned, e.g., by the POD-functions U_ψ^1 of the diode S_1 and U_ψ^2 of the diode S_2 respectively, by

$$d(U^1, U^2) := \max_{\substack{u \in U^1 \\ \|u\|_2 = 1}} \min_{\substack{v \in U^2 \\ \|v\|_2 = 1}} \|u - v\|_2.$$

Exploiting the orthonormality of the bases U_ψ^1 and U_ψ^2 and using a Lagrange framework, we find

$$d(U^1, U^2) = \sqrt{2 - 2\sqrt{\lambda}},$$

where λ is the smallest eigenvalue of the positive definite matrix $SS^\top$ with $S_{ij} = \langle u_{\psi,i}^1, u_{\psi,j}^2 \rangle_2$. The distances for the rectifier network are given in Table 2. While the reduced model for the diodes S_1 and S_3 are almost equal, the models for the diodes S_1 and S_2 are significantly different. Similar results are obtained for the reduction of n, p, etc.
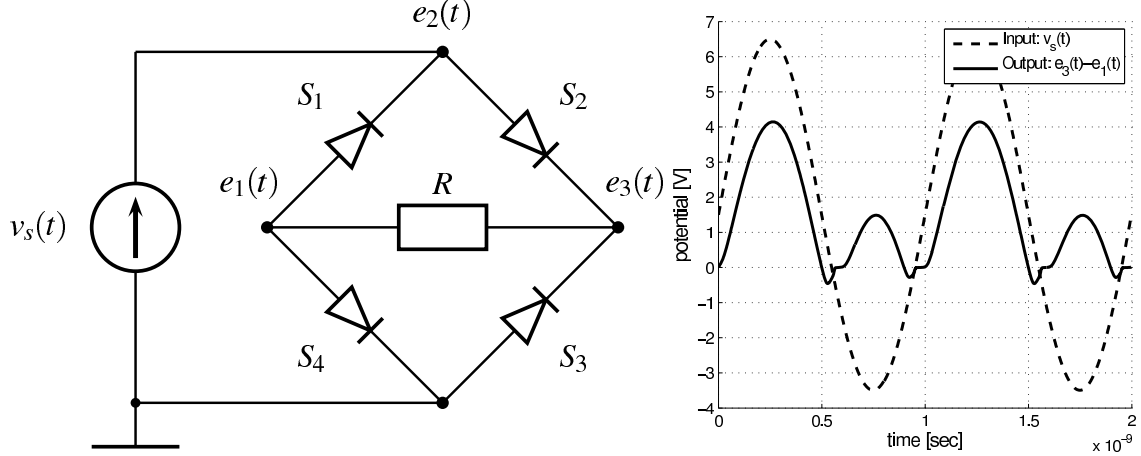

Fig. 7 Rectifier network and simulation results. The input v_s is sinusoidal with offset $+1.5[V]$.

Table 2 Distances between reduced models in the rectifier network.

Δ	$d(U^1, U^2)$	$d(U^1, U^3)$
10^{-4}	0.61288	$5.373 \cdot 10^{-8}$
10^{-5}	0.50766	$4.712 \cdot 10^{-8}$
10^{-6}	0.45492	$2.767 \cdot 10^{-7}$
10^{-7}	0.54834	$1.211 \cdot 10^{-6}$

Appendix: Proper Orthogonal Decomposition (POD)

Let $y : \Omega \times [0,T] \to \mathbb{R}$ be a function, which in the situation of Section 4 represents the time continuous finite element approximation of ψ, n, p, g_ψ, J_n and J_p, respectively. For $t \in [0,T]$ let $y(\cdot,t) \in Y_N := \mathrm{span}\{\phi_1,\ldots,\phi_N\}$, where ϕ_i $(i = 1,\ldots,N)$ denote linearly independent elements of a Hilbert space X.

The snapshot variant of POD introduced in [13] works as follows; let $Y = [y^1,\ldots,y^l] \in \mathbb{R}^{N \times l}$ contain as columns the coefficient vectors of l time-snapshots $y(\cdot,t_i)$ taken at time instances $t_i \in [0,T]$, i.e.

$$y(\cdot,t_i) = \sum_{j=1}^{N} y^i_j \phi_j.$$

Furthermore, let $M := (\langle \phi_m, \phi_n \rangle_X)_{m,n=1,\ldots,N}$ with its Cholesky factorization $M = LL^\top$. Let $(\tilde{U},\Sigma,\tilde{V})$ denote the singular value decomposition of $\tilde{Y} := L^\top Y$, i.e. $\tilde{Y} = \tilde{U}\Sigma\tilde{V}^\top$ with $\tilde{U} \in \mathbb{R}^{N \times N}$, $\Sigma \in \mathbb{R}^{N \times l}$, and $\tilde{V} \in \mathbb{R}^{l \times l}$ and Σ a diagonal matrix containing the singular values $0 \leq \sigma_i$ in decreasing order for $1 \leq i \leq l$, where we assume $l \leq N$. We set

$$U := L^{-\top}\tilde{U}_{(:,1:k)} \equiv [u^1,\ldots,u^k]. \tag{17}$$

Then, the k-dimensional POD basis of $\mathrm{span}\{\sum_{j=1}^{N} y^i_j \phi_j,\ i = 1,\ldots,l\} \subseteq Y_N$ is given by

$$\mathrm{span}\{\sum_{j=1}^{N} u^i_j \phi_j,\ i = 1,\ldots,k\}.$$

Note that one chooses $k \leq m$, where $\sigma_m > 0$ denotes the smallest non-vanishing singular value. The expression $1 - \Delta(k)^2$ is a measure of the information content of the subspace spanned by the first k POD basis functions, where

$$\Delta(k) = \sqrt{1 - \frac{\sum_{i=1}^{k} \sigma_i^2}{\sum_i^l \sigma_i^2}}. \tag{18}$$

References

1. Bodestedt, M., Tischendorf, C.: PDAE models of integrated circuits and index analysis. Math. Comput. Model. Dyn. Syst. **13**(1), 1–17 (2007)
2. Estévez Schwarz, D., Feldmann, U., März, R., Sturtzel, S., Tischendorf, C.: Finding beneficial DAE structures in circuit simulation. Jäger, Willi (ed.) et al., Mathematics – key technology for

the future. Joint projects between universities and industry. Berlin: Springer. 413-428. (2003)

3. Estévez Schwarz, D., Tischendorf, C.: Structural analysis of electric circuits and consequences. Int. J. Circuit Theory Appl. **28**(2), 131–162 (2000)

4. Gummel, H.: A self-consistent iterative scheme for one-dimensional steady state transistor calculations. Electron Devices, IEEE Transactions on **11**(10), 455–465 (1964)

5. Günther, M.: Partielle differential-algebraische Systeme in der numerischen Zeitbereichsanalyse elektrischer Schaltungen. VDI Fortschritts-Berichte, Reihe 20, Rechnerunterstützte Verfahren, Nr. 343 (2001)

6. Kahlbacher, M., Volkwein, S.: Galerkin proper orthogonal decomposition methods for parameter dependent elliptic systems. Discuss. Math., Differ. Incl. Control Optim. **27**(1), 95–117 (2007)

7. Markowich, P.: The Stationary Semiconductor Device Equations. Computational Microelectotrnics. Springer-Verlag Wien-New York. (1986)

8. Patera, A., Rozza, G.: Reduced Basis Approximation and A Posteriori Error Estimation for Parametrized Partial Differential Equations. Version 1.0. Copyright MIT 2006–2007, to appear in (tentative rubric) MIT Pappalardo Graduate Monographs in Mechanical Engineering. (2007)

9. Petzold, L.R.: A description of DASSL: A differential/algebraic system solver. IMACS Trans. Scientific Computing **1**, 65–68 (1993)

10. Selberherr, S.: Analysis and Simulation of Semiconductor Devices. Springer-Verlag Wien-New York. (1984)

11. Selva Soto, M.: A coupled system for electrical circuits. Numerical simulations. PAMM **6**(1), 51–54 (2006)

12. Selva Soto, M., Tischendorf, C.: Numerical analysis of DAEs from coupled circuit and semiconductor simulation. Appl. Numer. Math. **53**(2-4), 471–488 (2005)

13. Sirovich, L.: Turbulence and the dynamics of coherent structures I: Coherent structures. II: Symmetries and transformations. III: Dynamics and scaling. Q. Appl. Math. **45**, 561–590 (1987)

14. Tischendorf, C.: Coupled Systems of Differential Algebraic and Partial Differential Equations in Circuit and Device Simulation. Habilitation thesis, Humboldt-University of Berlin (2003)